

Experimental and theoretical studies of vibrational density of states in Fe₃O₄ single-crystalline thin films

B. Handke,² A. Kozłowski,¹ K. Parliński,³ J. Przewoźnik,¹ T. Ślęzak,¹ A. I. Chumakov,⁴ L. Niesen,⁵ Z. Kąkol,¹ and J. Korecki^{1,2}

¹*Faculty of Physics & Applied Computer Science, AGH University of Science and Technology, Kraków, Poland*

²*Institute of Catalysis & Surface Chemistry, Polish Academy of Sciences, Kraków, Poland*

³*The Henryk Niewodniczański Institute of Nuclear Physics, Polish Academy of Sciences, Kraków, Poland*

⁴*European Synchrotron Radiation Facility, P.B. 200, F-38043 Grenoble, France*

⁵*Nuclear Solid State Physics, Material Science Center, University of Groningen, Nijenborg 4, 9747 AG Groningen, The Netherlands*

(Received 15 May 2004; revised manuscript received 17 December 2004; published 7 April 2005)

This paper presents experimental and theoretical studies of lattice vibrations in a single-crystalline Fe₃O₄(001) thin film. The investigations were carried out in order to see how the lattice dynamics changes at the Verwey transition. Vibrational densities of states (DOS) were obtained from nuclear inelastic scattering (NIS) of synchrotron radiation in the temperature range 25 to 296 K, while theoretical DOS were calculated *ab initio* within density functional theory. Experimental phonon density of states shows good agreement with calculated DOS, reproducing both the general features of main line groups as well as the groups' structure. This is also in qualitative accord with heat capacity data, provided that experimental DOS is augmented with that calculated for oxygen atoms. We have observed a gradual change in the NIS raw data as well as the relevant DOS while lowering the temperature. In particular, the main peak in the energy region 15–25 meV shows increasing splitting on cooling. The Lamb-Mössbauer factor calculated in the course of DOS evaluation shows a pronounced drop in the vicinity of the Verwey transition that may be partly connected to the observed abrupt lowering of the count rate at approximately 7 meV for $T < T_V$. Since this is an indication of lattice stiffening below T_V , we conclude that we have found experimental evidence for lattice participation in the mechanism leading to the Verwey transition.

DOI: 10.1103/PhysRevB.71.144301

PACS number(s): 63.20.-e, 71.30.+h, 76.80.+y

I. INTRODUCTION

Magnetite (Fe₃O₄) is a mixed valence compound of the inverse spinel structure with the tetrahedral (*A*) sublattice occupied by ferric Fe³⁺ ions, and the octahedral (*B*) sublattice equally occupied by Fe²⁺ and Fe³⁺ ions. The distribution of iron ions at the octahedral sites is usually believed^{1,2} to change from dynamic disorder (“additional” electrons forming Fe²⁺ ions resonate between adjacent octahedral Fe³⁺ sites) to long-range order (resonating electrons get frozen) when lowering temperatures below $T_V = 125$ K. This transition (the Verwey transition) is accompanied by the latent heat, drastic drop of the dc conductivity, and the anomaly in most physical properties.³ Also, the crystal symmetry changes from cubic⁴ (*Fd3m*) to monoclinic (space group *Cc*).^{5,6}

This freezing electron picture was recently questioned by some measurements,^{7,8} and therefore the long-lasting controversy as to the origin of interactions leading to the transition is still an ongoing issue. The dominant interactions governing the transition were already discussed by Anderson,⁹ who showed that the electron motion is highly correlated due to interionic Coulomb interactions. However, Coulomb repulsion alone would cause the degeneration of any cationic pattern that develops below T_V . Therefore, some additional, although much weaker, interactions are required to stabilize long-range electronic order. Several possibilities for this additional driving force were proposed so far, e.g., electron-electron, electron-phonon, or magnetic interactions. Re-

cently, the dominant role of interionic Coulomb repulsion was questioned. For example, there is both experimental⁶ and theoretical¹⁰ evidence that the Anderson criterion, stating that each tetrahedron composed of octahedral Fe positions has equal number of Fe²⁺ and Fe³⁺ cations in order to minimize electrostatic energy, is violated. Therefore, the aim to find intervening interactions is even more vital. Here, we address the problem of a direct experimental check of lattice dynamics participating in the Verwey transition.

It is fairly well supported by the existing literature data that the lattice-electron coupling may contribute to the mechanism leading to the Verwey transition. First, the Verwey transition is accompanied by displacements of the ions, leading to a change in crystal symmetry. Also, the substitution of 43% of normal ¹⁶O by the heavier ¹⁸O isotope results in a considerable increase of T_V by approximately 5 K.¹¹ Finally, the transition in stoichiometric magnetite was shown to change its discontinuous character under the pressure of 6 GPa,¹² revealing similar universal T_V vs p relation as was observed for Fe_{3(1-d)}O₄ and Fe_{3-x}M_xO₄ (M=Zn or Ti) while changing the nonstoichiometry parameter d or doping level x .^{13,14}

Some direct studies of lattice dynamics were also done in the past. In particular, the quasielastic diffuse neutron scattering was observed by Shapiro *et al.*,¹⁵ also at q vectors incommensurate with low temperature structure, and extending up to 80 K above T_V . This phenomenon reflects fluctuating atomic positions of the frequency approximately 1–2 THz extending coherently throughout the lattice (i.e., not of

a localized character).¹⁶ Diffuse scattering diminishes abruptly as T falls below T_V ,¹⁷ and a similar behavior is observed in heat capacity data;¹⁸ here, the lattice contribution is reduced below T_V , indicating low temperature lattice stiffening. Even though no clear change in the phonon dispersion relation at low energies at T_V was reported, based on neutron inelastic scattering measurements,¹⁹ it should be noted that the authors used natural crystals with uncontrolled nonstoichiometry and/or dopant level, that may blur any subtle phenomena (see, e.g., Refs 13 and 14 for an extensive discussion of the influence of nonstoichiometry and doping on the Verwey transition). On the other hand, recent infrared and Raman studies do show some phonon stiffening: T_{2g}^3 , T_{2g}^2 , and A_{1g} modes move from 37.4, 67.07, and 82.94 meV at T just above T_V to 38.56, 67.82, and 83.32 meV just below the transition temperature, as reported in Ref. 20. According to Gasparov,²¹ the A_{1g} mode changes its position from 82.7 meV at 300 K to 83.9 meV at 5 K. Finally, quite recently, Seto *et al.*²² used a doped magnetite polycrystalline sample to test the new method to obtain site-specific phonon densities of states from the combination of nuclear resonance scattering in the time and energy domain. Accordingly, the partial phonon DOS at room temperature could be obtained and decomposed into contributions from tetrahedral and octahedral Fe sites.

In order to directly study the problem of lattice dynamics in magnetite at low energies, which can reflect the processes related to the Verwey transition, and on well-characterized single crystal, we have performed high-resolution nuclear inelastic scattering (NIS) measurements in a molecular beam epitaxy (MBE) grown Fe_3O_4 single-crystalline thin film as a function of temperature. The NIS method has been chosen because it probes vibrations at iron sites where the transition is supposed to originate; we have thus expected to gain direct information about iron lattice participation in the Verwey transition.

We have found reasonable agreement of the density of states drawn from experimental data with those calculated *ab initio* within density functional theory. We have observed a discontinuity at T_V as well as the gradual shift of the density of states to higher energies on cooling. These findings suggest that the lattice becomes more rigid below the Verwey transition.

Sample preparation, experimental procedures, and the methodology of DOS calculation are described in the next section. In Sec. III the results of measurements are presented, followed by the results of DOS calculations in Sec. IV and the discussion in Sec. V.

II. EXPERIMENTAL AND COMPUTATIONAL DETAILS

A. Sample preparation and characterization

The sample was an epitaxial (001) magnetite thin film grown on $\text{MgO}(001)$ enriched with ^{57}Fe to 95%. The polished $\text{MgO}(001)$ $10 \times 10 \times 1$ mm³ substrate was annealed for 1 h at 900 K in UHV (base pressure 1×10^{-8} Pa) to ensure atomic cleanness and the perfect structure of the exposed surface. The 500 nm film was grown by oxygen-assisted MBE at the O_2 partial pressure 5×10^{-4} Pa at the rate of

about 1 nm/min. During the deposition process, the substrate was kept at a constant temperature of 250 °C. The growth was *in situ* controlled by a quartz crystal monitor, low electron energy diffraction, (LEED), and conversion electron Mössbauer spectroscopy (CEMS). The freshly prepared film displayed a typical LEED pattern indicating the $(\sqrt{2} \times \sqrt{2})R45$ surface reconstruction, relative to the primitive surface unit cell of the $\text{Fe}_3\text{O}_4(001)$ face. The CEMS measurement revealed a spectrum typical for bulk stoichiometric magnetite. Moreover, the *ex situ* temperature CEMS (Ref. 23) and dc magnetization²⁴ measurements confirmed the occurrence of the Verwey transition at $T > 120$ K, indicating nearly perfect stoichiometry.

Temperature-dependent x-ray diffraction (XRD) measurements in the temperature range 70–300 K were performed on a Siemens D5000 diffractometer equipped with the OXFORD continuous flow cryostat and a rear graphite monochromator using $\text{Cu K}\alpha$ radiation. Patterns were collected after stabilizing the temperature of the sample for 30 min. The measurements were performed in order of increasing temperature after cooling the samples to below 70 K. The XRD patterns were fitted using the FULLPROF (Ref. 25) program, assuming a pseudo-Voigt function for peak shape and a polynomial function for the background intensity.

Diffraction was obtained from lattice planes parallel to the film surface so only peaks of the $(0\ 0\ l)$ type were observed and only $(0\ 0\ 4)$ and $(0\ 0\ 8)$ peaks of Fe_3O_4 and $(0\ 0\ 2)$ and $(0\ 0\ 4)$ peaks of MgO substrate crystal were measured (indexed on the base of the cubic unit cell). Below the Verwey transition temperature two additional weak $(0\ 0\ 3)$ and $(0\ 0\ 5)$ peaks, which are forbidden for cubic symmetry, were observed. The temperature dependence of the $(0\ 0\ 3)$ peak is shown in Fig. 1, which clearly indicates the onset and width of the Verwey transition.

B. Nuclear inelastic scattering of synchrotron radiation

NIS measurements were performed at the Nuclear Resonance beamline ID 18 (Ref. 26) in the European Synchrotron Radiation Facility (ESRF) in Grenoble, France. In this technique²⁷ synchrotron radiation incident photons, slightly off resonance in comparison with the ^{57}Fe nucleus excitation energy, E_0 , can be resonantly absorbed by the nucleus provided that the energy is exchanged with lattice vibrations. Thus, if a photon of energy $E_0 + \Delta E$ ($E_0 - \Delta E$) is absorbed, then the phonon of energy ΔE is created (or annihilated). The inelastic scattering is measured by detecting the yield of the delayed de-excitation products (mainly 6.4 keV $K\alpha$ fluorescence x rays from the internal nuclear conversion) as a function of the incidence beam energy.

A high-intensity synchrotron x-ray beam is monochromized by two successive monochromators²⁸ to the resonance energy E_0 (approximately 14.4 keV) of the ^{57}Fe nuclear Mössbauer transition. The design of the high-resolution monochromator²⁹ allows the adjustment of the incident energy by ± 80 meV from E_0 with the resolution of $\delta E = 0.65$ meV. The beam is then collimated by two sets of collimators, resulting in a focal spot of about 100×200 μm^2 on the sample position. The flux of the inci-

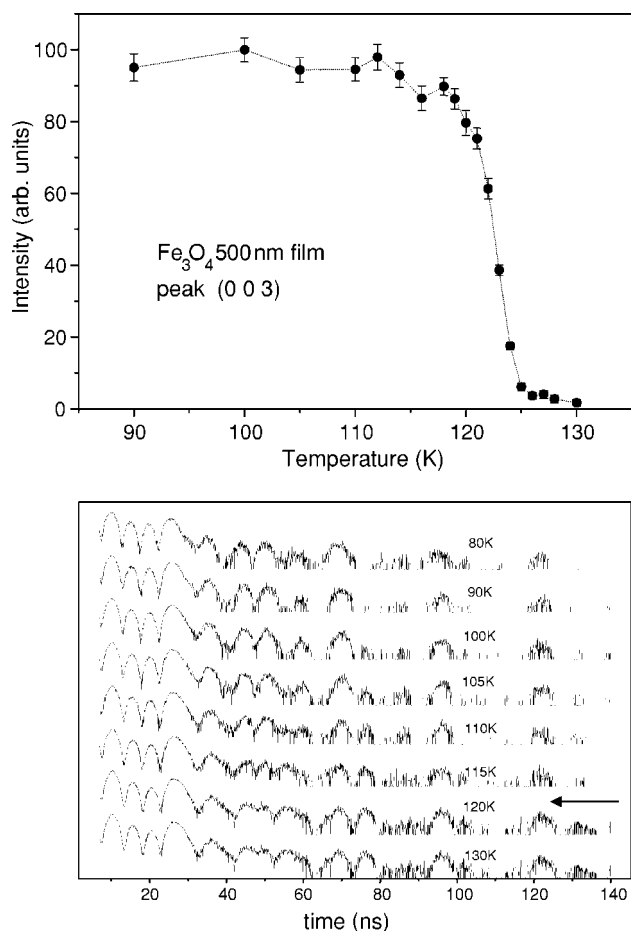


FIG. 1. Top: Variation of the (0 0 3) “forbidden” peak intensity while temperature rising for Fe_3O_4 single-crystalline thin film, where it is clear that the transition region extends from 125 K down to 120 K. Bottom: Time nuclear forward scattering (NFS) spectra taken for temperature range from 80 to 130 K. The arrow indicates the temperature region, 115 to 120 K, which corresponds to the Verwey transition.

dent radiation is monitored by an ionization chamber.

The delayed fluorescence photons are measured by an avalanche photodiode (APD) (Ref. 30) placed close to the sample to cover the largest possible solid angle. The second APD detector, located far from the sample, monitors coherent nuclear forward scattering (NFS). Those scattered quanta result from the collective de-excitation of the nuclei and form a narrow line around the resonance energy. This narrow line, whose width reflects the monochromatization process, constitutes the instrumental function. In order to optimize nuclear absorption in the thin magnetite film, the surface of the sample was inclined by $\sim 1^\circ$ relatively to the incident radiation. Because of the almost complete absorption of the incident radiation in the substrate, conventional simultaneous monitoring of the instrumental function in forward scattering was not possible. The monitoring of the instrumental function with grazing incidence scattering³¹ was not suitable either, because this would require a much smaller incidence angle. Therefore, the instrumental function was monitored separately by measurements of nuclear forward scattering in $\alpha\text{-}^{57}\text{Fe}$ foil. These measurements were performed regularly

in between the inelastic scattering scans. Unfortunately, the obtained instrumental function was not entirely identical to that during inelastic scattering measurements, which caused some problems in data processing, as discussed below.

The Fe_3O_4 thin film specimen was mounted on the tail of a closed-cycle refrigerator placed on a high-precision six-circle diffractometer cradle. The sample temperature was monitored by a Cernox thermometer placed 2–3 mm from the sample. The incidence beam was aligned at room temperature along the [100] Fe_3O_4 crystallographic direction of the sample. Measurements along the [110] direction at 25 K were also performed to find possible anisotropy of inelastic nuclear resonance scattering. Since the spectrum was virtually the same as that along [100], this result will not be further analyzed. Before the experiment the sample was cooled down to 25 K in an external magnetic field of approximately 0.3 T provided by permanent magnets. This procedure was aimed at establishing the unique easy magnetic axis of the low temperature magnetite phase²⁴ that is a necessary condition to avoid twinning of a c axis and to achieve the simplest possible structural-domain pattern.³²

The energy range studied was $\Delta E = -80$ up to $+80$ meV (“long scans”) for temperatures 25, 100, 120, 140, and 295 K. Additionally, short energy scans (-5 to 30 meV) at 80, 95, 105, 110, 115, and 130 K were made to precisely trace the changes in lattice dynamics close to the transition. At each temperature, the data were collected in several energy scans, lasting half an hour each. The average count rate in the intensity maximum of the inelastic part was 50 counts per second. The data were then added up and normalized. To initially separate regions above and below the Verwey transition we first carried out time-domain NFS measurements every 5 K in the vicinity of the predicted T_V . The results are shown in the inset of Fig. 1. Above the Verwey transition the spectra are similar to those reported by Kalev and Niesen³³ at room temperature. The changes observed in the NFS spectra by crossing the Verwey transition reflect the corresponding evolution of the Mössbauer spectrum.²³ Due to complexity of the magnetic moment alignment and the insufficient statistic in these auxiliary data, no further analysis was performed.

Nuclear inelastic scattering data were processed and the density of states was drawn following the procedure described by Kohn *et al.*^{34,35} and by Sturhahn *et al.*³⁶ and automated in the computer program DOS22. Since the procedures are standard for NIS measurements, further details will be omitted here.

C. Methodology of vibrational DOS calculations

The *ab initio* calculations of the electronic structure of Fe_3O_4 were performed within density functional theory, using the GGA ultrasoft pseudopotentials³⁷ implemented in the VASP (Refs. 38–40) package. We have used the crystallographic face-centered cubic supercells containing 56 atoms. The Brillouin zone integration was confined to a $2 \times 2 \times 2$ wave vector mesh. The calculated lattice constant was 8.4358 Å and the free structural parameter of oxygen in the reduced coordinates (x, x, x) was very close to 1/4,

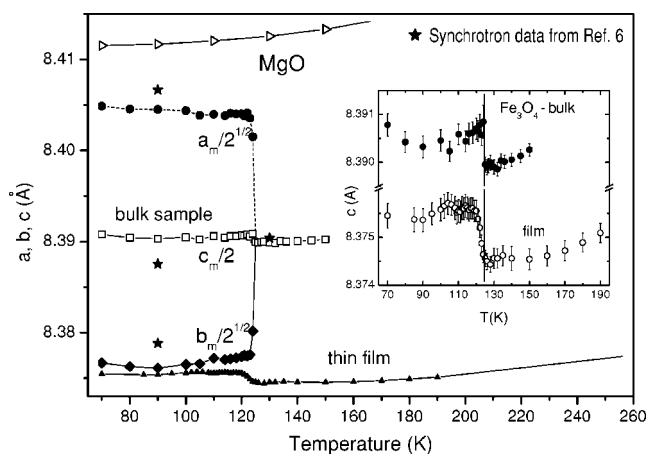


FIG. 2. Temperature dependence of the out-of-plane lattice parameter (solid triangles: cubic c for $T > T_V$ and $c_m/2$ for $T < T_V$) for Fe_3O_4 thin film obtained from the variation of the position of (0 0 4) and (0 0 8) reflections. The corresponding temperature dependence of the distorted cubic lattice parameters a ($=a_m/\sqrt{2}$, denoted by solid circles), b ($=b_m/\sqrt{2}$, solid diamonds), c ($=c_m/2$, open squares) for powdered Fe_3O_4 single crystal is also presented. The stars denote the relevant parameters obtained with the proper refinement from high-resolution XRD synchrotron measurements (Ref. 6). Note that the magnitude of the c parameter distortion is comparable to that obtained from our simplified refinement, but the sign is opposite. Finally, \triangleright symbols describe temperature dependence of doubled MgO lattice constant. The inset shows the expanded view of temperature variation of the cubic lattice parameter c for the thin film and the powder. The vertical line allows one to compare the Verwey transition temperature and the width of the transition for the thin film and the bulk.

namely $x=0.25520$. We confirmed the antiferromagnetic structure with magnetic moments equal to $-3.63 \mu_B$ and $3.65 \mu_B$ at tetrahedral and octahedral sites, respectively.

The phonon frequencies were determined by the direct method.⁴¹ Here, the Hellmann-Feynman forces were computed for positive and negative displacements with the amplitude of 0.03 \AA . All displaced configurations generate 1008 components of the Hellmann-Feynman forces. Next, the symmetry of the force constants, following from the $Fd\bar{3}m$ space group, were established and 121 independent parameters of so-called cumulant force constants were fitted to these forces by the singular value decomposition method.^{41–43} We have found that the force constant parameters diminish more than 2 orders of magnitude in the distance: supercell center–supercell surface. This provides reasonable phonon frequencies at all wave vectors. The largest force constant parameters are the on-site force constants (zero distance), while the smallest are located at the surface of the supercell. The force constants were used to construct the dynamical matrix, to diagonalize it, and to find the phonon frequencies. According to the direct method the exact phonon frequencies were obtained at high-symmetry points, Γ and X . These wave vectors are commensurate with the size of the supercell.

III. EXPERIMENTAL RESULTS

Before the NIS experiment the structural transition was monitored using x-ray diffraction. Our experimental proce-

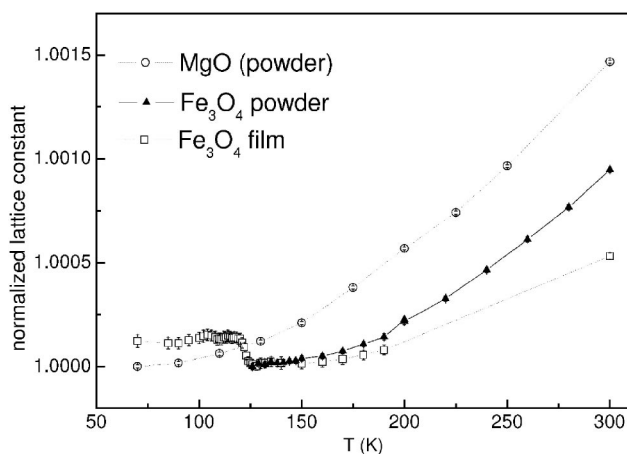


FIG. 3. Temperature dependence of normalized (to the value at T_V) cubic lattice constants for Fe_3O_4 and MgO powders compared to the normalized out-of-plane lattice parameter c for Fe_3O_4 thin film (same as presented in Fig. 2).

cedure of XRD does not enable observation of small monoclinic distortion expected in magnetite below T_V . Therefore, diffraction patterns collected below T_V were fitted assuming rhombohedral symmetry; unit cell parameters, a_m , b_m , c_m , and β , corresponding to hypothetical monoclinic Cc space group symmetry, were calculated using the formulas: $a_m = a_{rh} \sqrt{2(1 + \cos \alpha_{rh})}$, $b_m = a_{rh} \sqrt{2(1 - \cos \alpha_{rh})}$, $c_m = 2a_{rh}$, $\beta = \arccos[-\sqrt{2} \cos \alpha_{rh} / \sqrt{2(1 + \cos \alpha_{rh})}]$. Here, a_{rh} and α_{rh} are the relevant rhombohedral unit cell parameters. It should be noted that, although this procedure simplifies the refinement of diffraction data, it is nevertheless only approximate and may cause misleading conclusions, as discussed below.

In addition to the present thin film studies, the finely powdered high-quality single crystal of Fe_3O_4 (see Refs. 44 and 45 for the skull melter growth technique description and annealing conditions) was used for comparative XRD study of the bulk sample (using the same Siemens D5000 diffractometer). The results of temperature variation of lattice parameters for powder and c parameter for thin film are shown in Fig. 2, and the inset shows the expanded view of $c(T)$ for both samples. Since out-of-plane cubic lattice parameter for the thin film transforms to the monoclinic $c_m/2$ below T_V , throughout the whole text and figures both these parameters will be referred to as “ c ”. In the main figure the doubled lattice constant of the MgO substrate is also presented, and it is clear from the comparison of it with the thin film lattice parameter that the MgO substrate exerts negative pressure on growing magnetite film. Based on the lattice constant difference between magnetite and MgO, approximately 0.02 \AA , and published pressure dependence of lattice parameters in magnetite,⁴⁶ this negative pressure may be estimated as approximately 2 GPa. Although this lattice expansion, larger than that caused by the Verwey transition, diminishes while cooling (see Fig. 3, where normalized lattice constants for MgO, bulk magnetite and thin magnetite film are shown), it is still substantial at T_V and may strongly affect the properties of the thin film. For example, the thin film lattice relaxes upon cooling in such a way that the c parameter depends on T much weaker than for the bulk sample, as shown in Fig. 3.

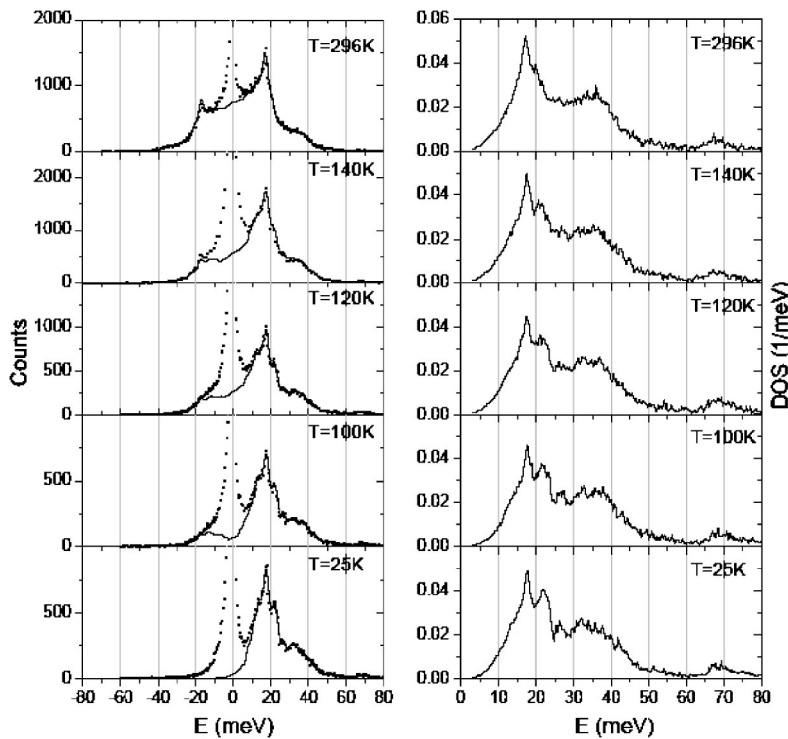


FIG. 4. (a) Raw data of nuclear inelastic scattering for various temperatures (dots) and with subtracted central peak (solid line). (b) Density of states extracted from NIS.

Also, as is clear from Fig. 2, the c parameter for the thin film increases when T drops below the Verwey transition, contrary to the bulk material (represented in Fig. 2 by the results of recent synchrotron studies⁶). Note that the expansion of c for the thin film was obtained directly from XRD, contrary to that for powder (\square symbols in Fig. 2), where a simplified procedure of refining a real magnetite monoclinic structure with rhombohedral symmetry also, artificially, leads to the increase of c below T_V . Finally, the finite width of the transition (from 118 to 126 K, as shown in the inset of Fig. 2), as opposed to the very sharp one in bulk, may be due to the substrate. Usually, application of pressure to magnetite diminishes the Verwey transition temperature.¹² We expect a similar effect in our case, even though the negative pressure is applied. Moreover, since the epitaxial strain is relaxed across the film, a T_V distribution, reflecting pressure variation, may appear.

Summarizing this section, the XRD analysis proved that the quality of our thin film is very high, indicating, however, that peculiarities of the thin film may influence its physical properties. We therefore have to take into account that our NIS results can reveal both universal magnetite characteristics and those peculiar to the thin film.

The transition temperature in NIS experiment can be estimated from the sudden qualitative change of the time evolution of NFS below 120 K, as indicated by the arrow in the inset of Fig. 1. The difference, 5–10 K between this value and that inferred from the x-ray data, is due to the fact that the sample surface was exposed to thermal radiation from a kapton window in close vicinity of the sample.

The energy dependences of inelastic scattering obtained in “long scans” are presented in Fig. 4(a); here, both raw experimental data and the data after the elastic peak was subtracted are shown. It was found that the tails of the central

peak did not correspond to the tails of the measured instrumental function, which heavily affected DOS evaluation for low energies, $E < 3$ meV. As mentioned above, the instrumental function was monitored not in parallel with the measurements of nuclear scattering but separately. Accordingly, the shapes of the instrumental function and the elastic peak of nuclear scattering data were not absolutely identical. This caused some problems in elastic peak subtraction. In high-resolution NIS measurements, the elastic peak is typically 2 orders of magnitude higher than the level of inelastic scattering at low energy. Therefore, even a small inconsistency in shapes of the elastic peak and the instrumental function can lead to a noticeable uncertainty in the residual data. For this reason, we were not able to obtain reliable data of inelastic scattering (and, therefore, of the density of states) below 3 meV. On the other hand, the data above 3 meV were found to be essentially stable relative to possible uncertainties in the elastic peak subtraction.

The negative (annihilation) part of the spectrum gradually disappears for lower temperatures, as expected. Also, gradual changes in the character of the energy dependence of NIS, as observed clearly in the creation part, occur with lowering temperature. In particular, the main peak at approximately 18 meV shows pronounced splitting with the high-energy part shifting to still higher energies while temperature falls below 120 K. The density of states, evaluated as described above, is shown in Fig. 4(b). In accordance with raw data, Fig. 4(a), the high-energy part of the main peak gradually develops with lowering temperature and it moves slightly to higher energies. However, we do not have clear indication that this process has a discontinuity near T_V . At 120 K the small peak at 27 meV suddenly changes its shape. This effect cannot be removed by a simple change of central peak subtraction conditions, so we consider it as a genuine fact, possibly related

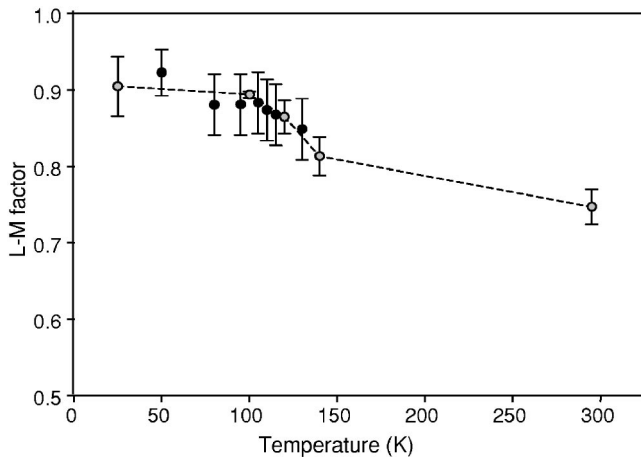


FIG. 5. Temperature dependence of Lamb-Mössbauer factor f_{LM} . Light-gray spots are the results of calculations from “long” scans and dark-gray spots from processed “short” scans. The dashed line is only to guide the eye.

to the Verwey transition. It also appears as if the center of gravity of the DOS line group around 36 meV at RT gradually shifts to lower energy with lowering temperature.

The temperature variation of the Lamb-Mössbauer factor, f_{LM} , calculated from the area of the normalized energy dependence, is presented in Fig. 5. The f_{LM} values calculated from “short” scans were also incorporated. The break at T_V is visible, indicating that the lattice becomes more rigid below T_V .

For short energy scans, since only the energy region from -5 to 30 meV was measured, we have extended the data to full region, -30 to 30 meV, using the detailed balance law. Consequently, the negative energy data $S(E)$ ($E < 0$) were taken as $S(E) = S(-E) / [\exp(-E/kT)]$ and the procedure was applied for E values beyond the main elastic maximum. The obtained spectrum was then smoothed in the energy region from -6 to -3 meV to assure continuity, and then DOS

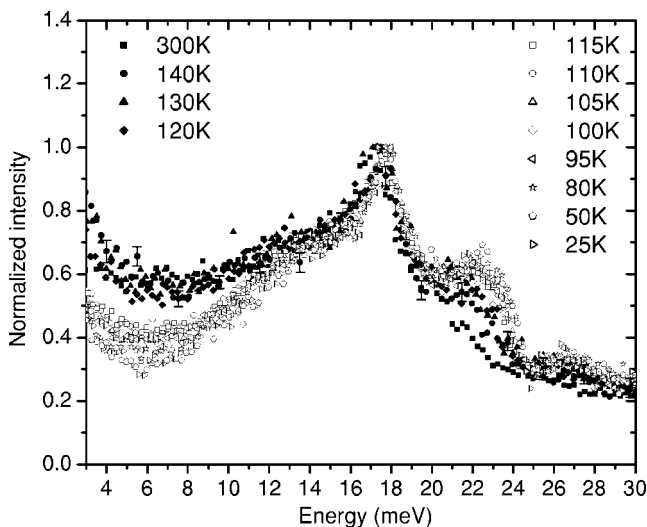


FIG. 6. Normalized (to the peak at 17 meV) raw data at a narrow energy range. Error bars, representative for all data points, are shown only for a few points for $T=140$ K for clarity.

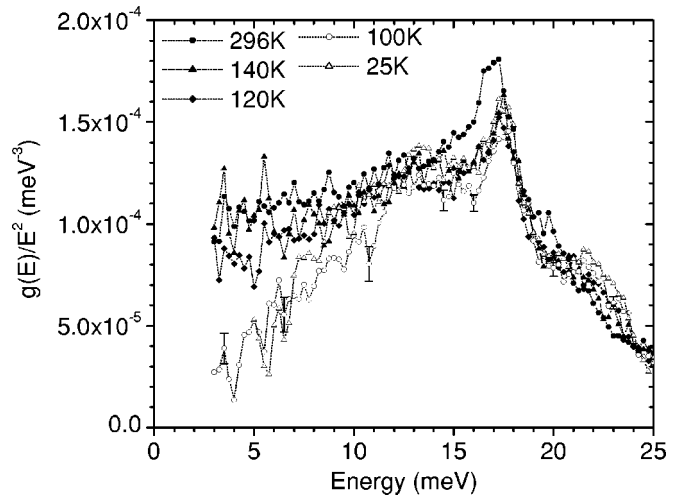


FIG. 7. Low-energy reduced DOS [as $g(E)/E^2$ vs E] calculated from long scans. Note that the usual quadratic density of states relation is approximately valid for high T up to about 10 meV, while no leveling off for low temperatures is seen down to 3 meV. Error bars, representative for all data points, are shown only for a few points for $T=100$ K for clarity.

curves were calculated as for long scans. This procedure, although definitely oversimplified, gave DOS that reflected major structure of the full analysis results. Since no new facts were found, these data are not presented here except for the f_{LM} factor calculation results in Fig. 5. However, interesting information can be gained by qualitative evaluation of the short scans. In Fig. 6 the low- E ($4 \text{ meV} < E < 30 \text{ meV}$) region of all experimental scans (short and long) normalized to the peak at 17 meV are presented. Clearly, the data are grouped in two sets corresponding to temperatures below ($T < 115$ K) and above ($T \geq 120$ K) the Verwey transition: the low-energy NIS is more intense for the high-temperature region. It looks like the spectral intensity is moved from the 22 meV region, where the decrease of the intensity is seen, to lower energies. In our opinion this is most probably linked to the diminishing of low- T phonon DOS, which may arise from the lattice suddenly stiffening at temperatures below T_V .

Low-energy density of states drawn from long scans is shown in Fig. 7. Here, the reduced DOS $g(E)/E^2$ vs E was presented to estimate the change of sound velocity at the transition. It is evident that the large difference between low- and high-temperature energy dependence exists, which will be further discussed below.

The low-energy phonon states were shown to be related to the diffuse scattering which had started already at approximately 200 K, and its temperature dependence revealed typical critical character.¹⁵ We cannot verify this trend here because of the narrow temperature range of our data (140 K down to 120 K). However, it is clear that the phenomena causing the increased intensity observed in Fig. 7 terminate at the transition, similar to the diffuse scattering. In our opinion, this effect should be further studied, e.g., by the precise low-energy transfer inelastic neutron scattering. As already pointed out, previous studies¹⁹ were not expected to show this phenomenon due to a possible large and uncontrolled nonstoichiometry.

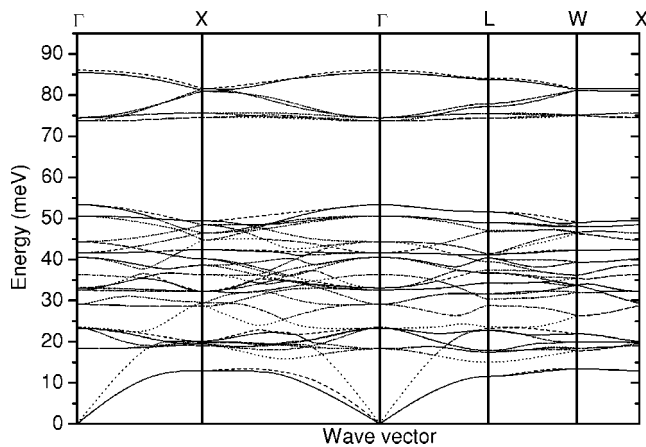


FIG. 8. *Ab initio* calculated phonon dispersion relation for Fe_3O_4 .

IV. RESULTS OF VIBRATIONAL DOS CALCULATIONS

The *ab initio* calculated phonon dispersion relations for the cubic structure $Fd\bar{3}m$ are shown in Fig. 8. They correspond to $T=0$ K. At low frequencies, the iron vibrations dominate while the high-frequency band comes mainly from oxygen. The low and high vibrational bands are separated by a gap of 21 meV. At the Γ point, modes of symmetry $T_{2g}(R)$ (29.1 meV) and $T_{1u}(I)$ (40.5 meV), being Raman and infrared active, respectively, originate from the vibrations of Fe atoms at the tetrahedral sites. The iron atoms at octahedral sites vibrate mainly in T_{2u} (18.3 meV), $T_{1u}(I)$ (23.3 meV), and A_{2u} (36.3 meV) modes. The phonon branches show considerable dispersion, which denotes that the interatomic interactions have a long-range order character. In agreement with the space group symmetry, all phonon modes at the X reciprocal lattice point are doubly degenerate.

As shown also by our diffraction experiment, the Verwey transition is accompanied by only negligible volume change and the very small shift of ionic positions.⁶ Moreover, our *ab initio* calculations have shown that in the cubic phase every atom resides in the local single minimum potential. This statement follows from the fact that the 3×3 on-site force constant matrix has all positive eigenvalues when bringing it into a diagonal form. In a crystal with a negative eigenvalue, a double minimum potential will appear, and subsequently it might cause a phase transition. If such a soft mode were to be found in the present calculations for $Fd\bar{3}m$, then some imaginary frequency should be observed. The unique relation between the high- and low-symmetry unit cells points at the wave vector $k_c = (0, 0, \frac{1}{4})/2a$, where the soft mode should occur. The same point at the wave number units related with the reciprocal lattice vectors is $q_c = (\frac{1}{4}, \frac{1}{4}, 0)$. This point occurs halfway between the Γ and X reciprocal lattice points. Our *ab initio* calculations did not show the existence of a soft mode,

even though it would be consistent with a critical scattering seen in neutron measurements,⁴⁷ as well as with elastic constant studies.^{48,49} There is also no mode of sufficiently low frequency to be a promising candidate for the soft mode. This, of course, does not exclude the possibility that the soft mode could appear if the strong electron-electron

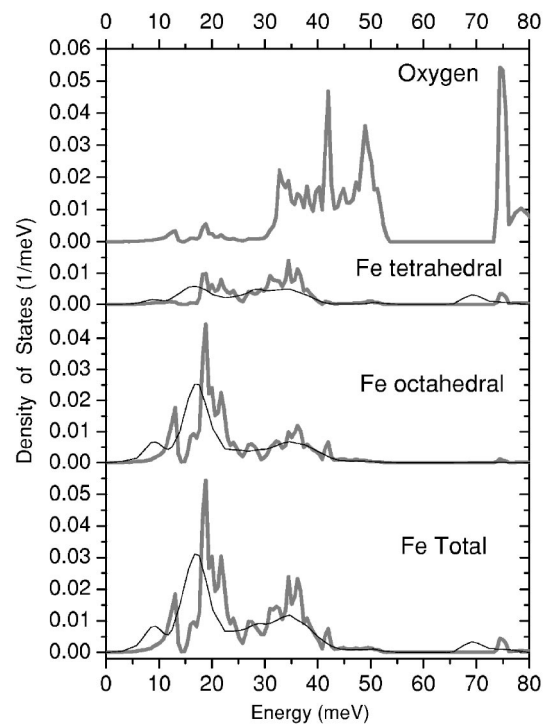


FIG. 9. *Ab initio* calculated phonon density of states for Fe_3O_4 . The thin line shows the relevant DOS calculated *ab initio* within density functional theory in Ref. 22.

interactions were more adequately included in the *ab initio* calculations.

Phonon density of states calculated from the phonon dispersion relation is presented in Fig. 9. The low-frequency part is due to iron vibrations. We observe a sharp peak at 12 meV, which is caused by the transverse acoustic phonon motion of Fe in the octahedral sites. The Fe atoms in tetrahedral sites remain relatively “silent” in the frequency range from zero to 15 meV. Hence, one may be sure that the additional intensity at low frequencies in the nuclear inelastic scattering measured at elevated temperatures, Figs. 6 and 7, is due to the octahedrally coordinated Fe atoms. The high-intensity double peaks occur at 18.6 and 21.7 meV. Successive peaks appear at 27, 32, 34.5, 36.1, and 42 meV. Starting from the 18.6 meV peak, the relative contribution from the tetrahedral Fe ions increases and for the sequence of peaks at frequencies higher than 25 meV, the contributions of Fe from tetrahedral and octahedral sites become comparable.

Similar phonon density of states of Fe has been recently obtained in Ref. 22 within the framework of the linear response perturbation method, and are included in Fig. 9 for comparison. All curves are shifted to lower energies as compared to our results. Apparently, similar conclusions as to the dominant role of octahedral iron atom vibrations at lowest energies may be drawn. Since the phonon frequencies were calculated in Ref. 22 only for eight irreducible wave vectors, and the resolution function of the monochromator was taken into account, phonon DOSs from Ref. 22 are slightly featureless and do not reproduce, e.g., the experimentally observed main peak splitting.

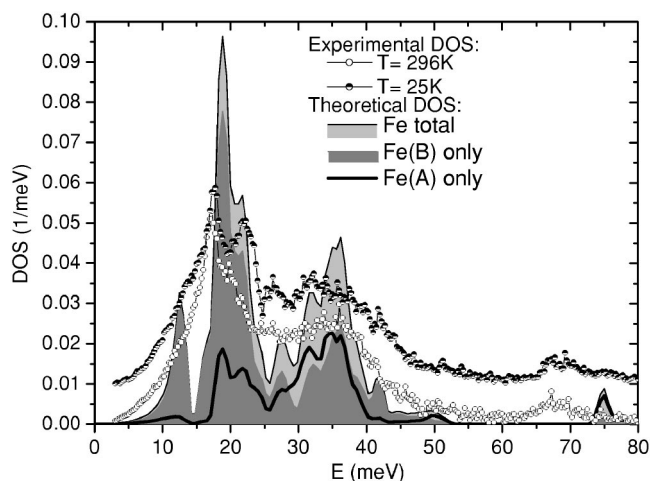


FIG. 10. Comparison of experimental DOS at 25 and 296 K with those calculated for both crystallographic positions (A—tetrahedral; B—octahedral) of Fe. Note that the experimental results for 25 K are shifted by 0.01 (meV)^{-1} .

The *ab initio* phonon calculations should be relevant to the nuclear inelastic scattering measured at the lowest temperature of $T=25 \text{ K}$. Of course, at this temperature the Fe_3O_4 structure is monoclinic, but the monoclinicity is small in comparison to typical structural phase transitions. Therefore, the overall phonon behavior of magnetite at low temperatures, and in particular of such integrated quantity as the phonon density of states, can be very well approximated by the phonon calculations in the cubic structure.

V. DISCUSSION

In Fig. 10 we have compared our experimental DOS at 300 and 25 K with those calculated *ab initio* and averaged within the region of approximately 1 meV to mimic experimental resolution. For calculated DOS, not only is the total Fe density of states shown but also partial DOS for octahedral and tetrahedral iron sublattices are presented. The main features of the experimental DOS—positions of the principal peak groups at 20 and 36 meV—are reproduced in calculations. Moreover, the splitting to particular lines has qualitatively similar character as those calculated. On the other hand, our results reveal a shoulder at approximately 13 meV, while the well-separated excitation of octahedral iron at 12 meV is predicted theoretically, and the same, but at lower energy, was found theoretically in the results presented in Ref. 22. Also, instead of the peak at around 68 meV as observed experimentally, the peak group at 75 meV, which is composed of tetrahedral iron and oxygen vibrations, is deduced from *ab initio* calculations.

Thus, the calculated DOSs for iron atoms are in qualitative agreement with our experimental results, and it can be unambiguously concluded that NIS for $E < 25 \text{ meV}$ is primarily due to octahedral iron sublattice vibration spectrum. The sudden change at T_V , which is clearly visible in Figs. 6 and 7, is related to the change of octahedral iron vibration occurring at the Verwey transition.

It is apparent that the experimentally determined DOS curves are considerably broadened in comparison with theoretical ones, even though the experimental resolution was taken into account. Real dispersion relation branches at room temperature are usually broadened²⁸ by about 2 meV due to phonon-phonon scattering caused by anharmonicity, the effect well reproduced by theoretical calculations.⁵⁰ Additional broadening due to lowering of phonon lifetime caused by disorder (either isotopic or structural inhomogeneities) can increase the total broadening to approximately 3–4 meV. Even with this broadening and also assuming damping effects as in Ref. 51, the most outstanding differences between experimental and theoretical DOS, especially at low energies, could not be removed.

The conclusion that NIS for the low-energy region is mainly due to octahedral iron was also drawn in Ref. 22. Finally, octahedral iron atoms were found to have the most extended fluctuations among all atoms in the recent combined neutron and x-ray scattering data,⁶ thus confirming indirectly low energy of intercationic interactions.

As shown in Fig. 7, a distinct difference between reduced DOS above and below T_V is seen. Notwithstanding the lack of low-energy data (below 3 meV), the slopes of $g(E)/E^2$ change to such extent that different reduced DOS values at $E=0$ are obvious. An interpolation of the reduced DOS to $E=0$ [with the assumption that $g(E)/E^2$ should level off] gives at least a factor of 2 difference between the data above and below the transition. This should correspond to at least a 25% increase (factor $2^{1/3}$) of a mean sound velocity below the transition.³⁴ The mean sound velocity (in this case) is mainly determined by the transversal component and, correspondingly, by the c_{44} elastic constant. In particular, the observed effect should correspond to approximately 50% (factor $2^{2/3}$) variation of c_{44} . It is, thus, much larger than expected from elastic constant measurements,⁴⁸ where the effect is only 15%. (Although, for technical reasons, the exact change in elastic constants across the transition could not be determined in Ref. 48.)

Experimental data showed that a pronounced dependence on temperature might result from anharmonicity. However, the predicted changes of the spectrum due to temperature dependence of anharmonicity effects are too small to explain the observed differences between 25 K and room temperature⁵² and are below the detection limit due to energy resolution of our technique. Thus, the change of energy dependence of inelastic absorption with temperature is due to other than anharmonicity effects, as we are discussing below.

Figure 11 shows our experimentally obtained DOS for room temperature, as well as DOS estimated from several existing literature data, in particular from Seto *et al.*'s²² nuclear inelastic scattering measurements on heavy doped (with 7 mol % Ni) magnetite polycrystal and room temperature inelastic neutron scattering.¹⁹ Also, peak positions in Raman scattering and optical data are marked for comparison.^{20,21,53,54} Both NIS results nearly coincide (except some shift of the results from Ref. 22 to higher energies; see the later discussion), which suggests that high-temperature vibrations of magnetite lattice are almost not

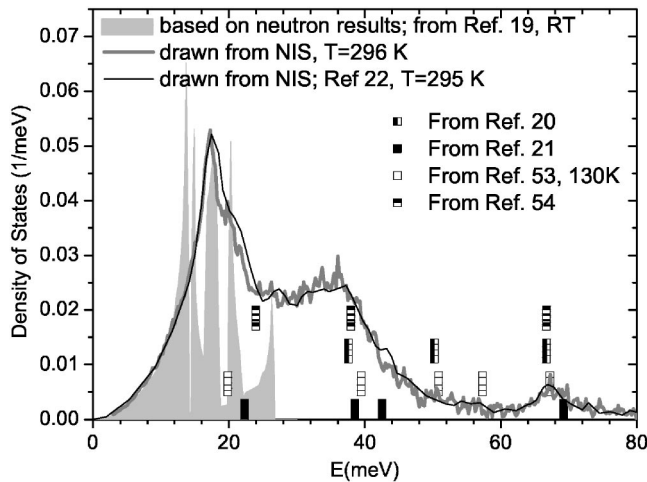


FIG. 11. Experimental DOS measured at 296 K in comparison with the results drawn from nuclear inelastic scattering at room temperature reported in Ref. 22, room temperature inelastic neutron studies (shaded), and literature data from optic studies (vertical bars; here, only peak positions are marked).

affected by the sample crystallinity, stoichiometry, and form, while the transition critically depends on the deviation from the ideal structure.

Neutron scattering data were processed assuming the spherical Brillouin zone, and that the dispersion relation does not appreciably depend on k direction. Although this calculation is oversimplified, which may primarily lead to an unrealistic peak height in the calculated DOS, the positions of DOS maxima are roughly consistent with those from our results. Only in the vicinity of $E \sim 13.5\text{--}15$ meV, and $E \sim 20.2$ meV, where neutron data have clear peaks in DOS, small shoulders are seen in our results at 295 K. The reason for this discrepancy is, most probably, the above-mentioned simplified derivation of DOS from neutron data. It is, however, interesting that the group of peaks in neutron DOS at $E \sim 13.5\text{--}15$ meV is well detached from the main peak at 17.5 meV, as in the theoretical DOS. Note, finally, that the cutoff in DOS derived from the neutron data comes from the lack of experimental points above 27 meV.

The peak at 17.2 meV and the shoulder at 19.8 meV, in our room temperature NIS spectrum, are shifted by about -0.5 meV with respect to the neutron data and also with respect to the data from Ref. 22. However, the neutron peak at 17.7 meV exactly coincides with the peak position of the 25 K spectrum. Since our measurements were performed on thin film, this shift might result from the MgO substrate influence on Fe_3O_4 sample. Indeed, if the negative pressure of 2 GPa is exerted on magnetite at room temperature due to MgO substrate, as discussed in Sec. III, then it may cause several shifts of vibration spectrum, not exceeding -2 meV, as, e.g., suggested by the pressure dependence of the $T_{2g}(2)$ mode shown in Ref. 54. Cooling to 25 K may relax this pressure, as discussed above, causing the spectrum shift, e.g., from 17.2 meV at room temperature to 17.7 meV at 25 K.

Our results show that the peak at 21 meV, at room temperature, moves to 23 meV at $T=25$ K, i.e., the lattice be-

comes more rigid when cooling. Samuelsen and Steinsvoll¹⁹ did not mention this fact: the data at temperatures below 119 K, the Verwey temperature of their sample, were basically the same as those measured at 300 K. Also, no indication of this pronounced lattice stiffening is suggested by the results of elastic constant studies on the single-crystalline bulk material.^{48,49}

Again, this shift might be due to the MgO substrate: the shift is 2 meV, i.e., it is still conceivable according to the estimated negative pressure. Then, however, the DOS for our “relaxed” sample, showing a peak at 23 meV, should be comparable to that of neutron data at room temperature. Since this is not the case—neutron and NIS peaks match very well at room temperature—the situation is probably more complicated.

Several literature reports show 10% softening of c_{44} mode above T_V .^{48,49} This softening should mainly affect X and Σ acoustic transverse modes resulting in only 0.5 meV energy shift. Those effects, however, may easily be masked by the influence of the MgO substrate, as mentioned earlier.

Summarizing the above discussion, we did not find drastic differences in density of states above and below the Verwey transition, although we had noticed that the peak at 21 meV develops and gradually moves to 23 meV with decreasing temperature. In addition, the low-energy 4–12 meV spectrum differs for $T < T_V$ and $T > T_V$ (with a discontinuity at T_V), which may be due to lattice stiffening.

Since a lattice stiffening below T_V was suggested in the paper presenting heat capacity data,¹⁸ it is natural to use our experimentally obtained DOS (only from long scans) to calculate the lattice heat capacity C_L and compare it with our experimental results. At a given temperature, C_L is proportional to the value obtained from the formula⁵⁵

$$C_L \propto \int_0^\infty \left(\frac{h\nu}{2k_B T} \right)^2 \left(\frac{2 \exp\left(-\frac{h\nu}{2k_B T}\right)}{1 - \exp\left(-\frac{h\nu}{k_B T}\right)} \right)^2 g(\nu) d\nu,$$

where $g(\nu)$ is temperature dependent. The experimental Fe DOS extracted from NIS experiment was supplemented with the theoretical oxygen DOS and we assumed it is temperature independent. Results from our calculations are shown in Fig. 12, together with the experimental data from Ref. 18, complemented with higher temperature measurements. Since we have only five representative density of states sets, the same set is used for several temperatures, as marked in Fig. 12; as a result the clear steps in the $C_L(T)$ relation occur at temperatures on the boundaries.

Taking into account all simplifications (oxygen density of states were calculated at $T=0$ K; only five temperatures where experimental DOS was measured; constant volume

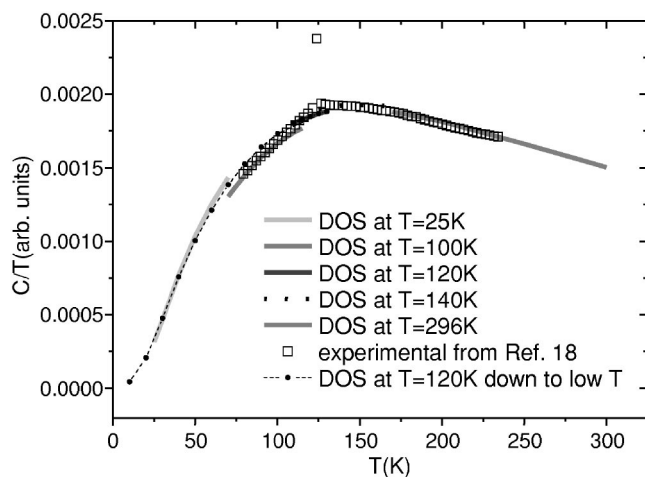


FIG. 12. Lattice heat capacity calculated from experimental DOS supplemented with calculated DOS for oxygen atoms.

lattice specific heat is calculated and the constant pressure specific heat is measured), the agreement between the shape of experimental heat capacity and that calculated from NIS experiment is very good. It is thus clear that basically all major contributions to lattice vibration were revealed by the experiment and taken into account in oxygen DOS calculation. It was found in Ref. 18 that a drastic change of lattice specific heat occurs at T_V when the transition is approached from above. This change was suggested to be related to stoichiometric magnetite lattice stiffening below T_V in comparison to vibration spectrum at higher temperatures. Similar phenomena were observed in nonstoichiometric $\text{Fe}_{3(1-d)}\text{O}_4$ or doped magnetite $\text{Fe}_{3-x}\text{M}_x\text{O}_4$ ($\text{M}=\text{Zn}$ or Ti) for $3d=x < 0.012$, i.e., where these materials undergo the discontinuous Verwey transition. Conversely, for higher defect concentration, $0.012 < 3d=x < 0.036$, where magnetite exhibits the Verwey transition of “second”⁵⁶ order, the lattice heat capacity was supposed to remain intact by the transition. To verify this idea, i.e., the lattice origin of the different low- and high- temperature specific heat dependence, we have included in Fig. 12 the low-temperature ($T < T_V$) lattice specific heat calculated from DOS measured at 120 K, i.e., above T_V . The discrepancy between these results and those calculated from DOS measured, e.g., at 100 K, is marginal. This clearly shows that the interpretation from Ref. 18 is not justified: no major alteration of vibrational DOS is needed to account for the C_L vs T relation. The problem still remains why C_L for magnetite exhibiting the second-order transition is so distinctly different from that for the first order.

It may be argued that some anomaly in phonon spectrum should always be present at the temperature where a structural phase transition takes place. As already mentioned, the Verwey transition is accompanied by structural transformation from high-temperature cubic to monoclinic, and some reconstruction of lattice dynamics certainly occurs. However, our preliminary *ab initio* calculations showed that such a small distortion would not produce any changes in vibrational DOS if not accompanied by modifications in electronic structure. Also, a similar alteration of structure (although not of discontinuous character) is observed in

nonstoichiometric and doped magnetite undergoing a “second”-order Verwey transition. However, the contribution to neutron intensity from diffuse scattering, the effect related to lattice vibration, does not terminate at T_V ¹⁷ and different changes of lattice heat capacity¹⁸ below T_V are observed. This suggests that the temperature dependence of lattice dynamics that we have encountered is closely related to the Verwey transition of the first order, and that electron-lattice interactions affect the order of the Verwey transition.

VI. CONCLUSIONS

We have presented the results of experimental and theoretical studies of lattice vibrations in single-crystalline Fe_3O_4 film MBE grown on MgO . Theoretical density of states were calculated *ab initio*, together with electronic structure, within density functional theory, using the GGA ultrasoft pseudopotentials. Phonon density of states drawn from nuclear inelastic scattering data show good coincidence with calculated DOS for iron, reproducing both the general feature of main line groups as well as the groups’ structure. Experimental DOS also explains our heat capacity results, provided that NIS DOS is augmented with that calculated for oxygen atoms.

We have observed the continuous change of vibrational DOS with temperature, which suggests lattice stiffening at lower temperature. Although the character of main changes does not clearly indicate that this process takes place at T_V , some shift to higher energy of vibration energy spectrum and the abrupt intensity change in low energy DOS, was found at T_V . Additionally, the Lamb-Mössbauer factor increases abruptly below the transition. These two effects indicate the direct relation between the Verwey transition and phonons in stoichiometric magnetite single crystal, as also recently postulated by Subias *et al.*⁵⁷ Neglecting the electron-phonon interaction may lead to the apparent discrepancy between the experimental results⁵⁷ claiming no charge ordering and recent LDA+U calculations^{58,59} revealing the charge ordering.

The temperature dependence of the experimental DOS above T_V does not reveal lattice softening, nor does the calculated electronic structure indicate any possibilities of soft mode formation. But, the softening mode is the experimental fact found in elastic constant studies. And, although due to possible influence of MgO substrate we cannot expect this phenomenon to be clearly revealed by our experiment on thin film, it should be predicted by theoretical studies. Since this is not the case, we think that not all important interactions are incorporated in the calculations. We hope that the improved calculations, with the more realistic description of electronic correlations, might eventually lead to better agreement with the experimental data.

ACKNOWLEDGMENTS

This work is financially supported by the KBN State Committee for Scientific Research. Financial support by The Foundation for Polish Science (FNP) is also kindly acknowledged.

- ¹E. J. Verwey, *Nature (London)* **144**, 327 (1939).
- ²F. Walz, *J. Phys.: Condens. Matter* **14**, R285 (2002).
- ³Z. Kałkol, *J. Solid State Chem.* **88**, 104 (1990).
- ⁴W. C. Hamilton, *Phys. Rev.* **110**, 1050 (1958).
- ⁵M. Iizumi, T. F. Koetzle, G. Shirane, C. Chikazumi, M. Matsui, and S. Todo, *Acta Crystallogr., Sect. B: Struct. Crystallogr. Cryst. Chem.* **38**, 2121 (1982).
- ⁶J. P. Wright, J. P. Attfield, and P. G. Radaelli, *Phys. Rev. B* **66** 214422 (2002).
- ⁷P. Novak, H. Stepankova, J. Englich, J. Kohout, and V. A. M. Brabers, *Phys. Rev. B* **61**, 1256 (2000).
- ⁸J. Garcia, G. Subias, M. G. Proietti, J. Blasco, H. Renevier, J. L. Hodeau, and Y. Joly, *Phys. Rev. B* **63**, 054110 (2001); J. Garcia, and G. Subias, *J. Phys.: Condens. Matter* **16**, R145 (2004).
- ⁹P. W. Anderson, *Phys. Rev.* **102**, 1008 (1956).
- ¹⁰Z. Szotek, W. M. Temmerman, A. Svane, L. Petit, G. M. Stocks, and H. Winter, *Phys. Rev. B* **68**, 054415 (2003).
- ¹¹E. I. Terukov, W. Reichelt, D. Ihle, and H. Opperman, *Phys. Status Solidi B* **95**, 491 (1979).
- ¹²G. Kh. Rozenberg, G. R. Hearne, M. P. Pasternak, P. A. Metcalf, J. M. Honig, *Phys. Rev. B* **53**, 6482 (1996).
- ¹³J. P. Shepherd, J. W. Koenitzer, R. Aragón, J. Spalek, and J. M. Honig, *Phys. Rev. B* **43**, 8461 (1991).
- ¹⁴V. A. M. Brabers, F. Walz, and H. Kronmüller, *Phys. Rev. B* **58**, 14 163 (1998).
- ¹⁵S. M. Shapiro, M. Iizumi, and G. Shirane, *Phys. Rev. B* **14**, 200 (1976).
- ¹⁶K. Siratori, Y. Ishii, Y. Morii, S. Funahashi, S. Todo, A. Yanase, J. Phys. Soc. Jpn. **67**, 2818 (1998).
- ¹⁷R. Aragón, P. M. Gehring, and S. M. Shapiro, *Phys. Rev. Lett.* **70**, 1635 (1993).
- ¹⁸A. Kozłowski, Z. Kałkol, D. Kim, R. Zalecki, and J. M. Honig, *Phys. Rev. B* **54**, 12 093 (1996).
- ¹⁹E. J. Samuelsen and O. Steinsvoll, *Phys. Status Solidi B* **61**, 615 (1974).
- ²⁰R. Gupta, A. K. Sood, P. A. Metcalf, and J. M. Honig, *Phys. Rev. B* **65**, 104430 (2002).
- ²¹L. V. Gasparov, D. B. Tanner, D. B. Romero, H. Berger, G. Margaritondo, and L. Forró, *Phys. Rev. B* **62**, 7939 (2000).
- ²²M. Seto, S. Kitao, Y. Kobayashi, R. Haruki, Y. Yoda, T. Mitsui, and T. Ishikawa, *Phys. Rev. Lett.* **91**, 185505 (2003).
- ²³B. Handke, T. Ślęzak, M. Kubik, and J. Korecki, *J. Radioanal. Nucl. Chem.* **246**, 27 (2000).
- ²⁴A. Wiecheć, J. Korecki, B. Handke, Z. Kałkol, D. Fus, and A. Kozłowski, *Proceedings of the IX School of High T_c Superconductivity*, Krynica, Poland, 10–14 June (2001), edited by A. Szytuła and A. Kołodziejczyk (Acta Physica Polonica B Press, 2002), p. 241.
- ²⁵J. Rodriguez-Carvajal, *Physica B* **192**, 55 (1993). See <http://www-llb.cea.fr/fullweb/powder.htm>
- ²⁶R. Rüffer and A. I. Chumakov, *Hyperfine Interact.* **97–98**, 589 (1996).
- ²⁷M. Seto, Y. Yoda, S. Kikuta, X. W. Zhang, and M. Ando, *Phys. Rev. Lett.* **74**, 3828 (1995); A. I. Chumakov, R. Rüffer, A. Q. R. Baron, H. Grünsteudel, and H. F. Grünsteudel, *Phys. Rev. B* **54**, R9596 (1996); R. Röhlberger, W. Sturhahn, T. S. Toellner, K. W. Quast, E. E. Alp, A. Bernhard, J. Metge, and R. Rüffer, E. Burkel, *Physica B* **263–264**, 581 (1999).
- ²⁸A. I. Chumakov, W. Sturhahn, *Hyperfine Interact.* **123/124**, 781 (1999).
- ²⁹A. I. Chumakov, R. Rüffer, O. Leupold, A. Barla, H. Thiess, T. Asthalter, B. P. Doyle, A. Snigirev, and A. Q. R. Baron, *Appl. Phys. Lett.* **77**, 31 (2000).
- ³⁰A. Q. R. Baron, R. Rüffer, and J. Metge, *Nucl. Instrum. Methods Phys. Res. A* **400**, 124 (1997).
- ³¹R. Röhlberger, *Hyperfine Interact.* **123/124**, 455 (1999).
- ³²B. A. Calhoun, *Phys. Rev.* **94**, 1577 (1954).
- ³³L. A. Kalev and L. Niesen, *Phys. Rev. B* **67**, 224403 (2003).
- ³⁴V. G. Kohn, A. I. Chumakov, and R. Rüffer, *Phys. Rev. B* **58**, 8437 (1998).
- ³⁵V. G. Kohn, and A. I. Chumakov, *Hyperfine Interact.* **125**, 205 (2000).
- ³⁶W. Sturhahn, T. S. Toellner, E. E. Alp, X. Zhang, M. Ando, Y. Yoda, S. Kikuta, M. Seto, C. Kimball, and B. Dabrowski, *Phys. Rev. Lett.* **74**, 3832 (1995).
- ³⁷D. Vanderbilt, *Phys. Rev. B* **41**, 7892 (1990).
- ³⁸G. Kresse, J. Hafner *Phys. Rev. B* **47**, 558 (1993); **49**, 14 251 (1994).
- ³⁹G. Kresse and J. Furthmüller, *VASP Software*, Vienna (2002); <http://cms.mpi.univie.ac.at/CMSPage/main/>
- ⁴⁰G. Kresse, J. Hafner, *J. Phys.: Condens. Matter* **6**, 8245 (1994).
- ⁴¹K. Parlinski, Z.-Q. Li, and Y. Kawazoe, *Phys. Rev. Lett.* **78**, 4063 (1997).
- ⁴²K. Parlinski, *Am. Inst. Phys. Conference Proceedings 479*, Neutrons and Numerical Methods, edited by M. R. Johnson, G. J. Kearley, and H. G. Büttner, p. 121 (1999).
- ⁴³K. Parlinski, *PHONON Software*, Cracow (2003); <http://wolf.ifj.edu.pl/phonon/>
- ⁴⁴H. R. Harrison and R. Aragón, *Mater. Res. Bull.* **13**, 1097 (1978).
- ⁴⁵R. Aragón, H. R. Harrison, R. H. McCallister, and C. J. Sandberg, *J. Cryst. Growth* **61**, 221 (1983).
- ⁴⁶A. Kuriki, Y. Moritomo, Y. Ohishi, K. Kato, E. Nishibori, M. Takata, M. Sakata, N. Hamada, S. Todo, N. Mori, O. Shimomura, and A. Nakamura, *J. Phys. Soc. Jpn.* **71**, 3092 (2002).
- ⁴⁷Y. Fujii, G. Shirane, and Y. Yamada, *Phys. Rev. B* **11**, 2036 (1975).
- ⁴⁸H. Schwenk, S. Bareiter, C. Hinkel, B. Lüthi, Z. Kałkol, A. Kozłowski, and J. M. Honig, *Eur. Phys. J. B* **13**, 491 (2000).
- ⁴⁹T. J. Moran, and B. Lüthi, *Phys. Rev.* **187**, 710 (1969).
- ⁵⁰J. Menéndez and M. Cardona, *Phys. Rev. B* **29**, 2051 (1984).
- ⁵¹R. Röhlberger, W. Sturhahn, T. S. Toellner, K. W. Quast, P. Hession, M. Hu, J. Sutter, and E. E. Alp, *J. Appl. Phys.* **84**, 584 (1999).
- ⁵²A. Debernardi, *Solid State Commun.* **113**, 1 (1999).
- ⁵³L. Degiorgi, I. Blatter-Morke, and P. Wachter, *Phys. Rev. B* **35**, 5421 (1987).
- ⁵⁴O. Shebanova and P. Lazor, *J. Chem. Phys.* **119**, 6100 (2003).
- ⁵⁵E. S. R. Gopal, *Specific Heats at Low Temperatures* (Heywood, London, 1966).
- ⁵⁶The existence of a long-range order for highly doped and nonstoichiometric magnetite was not confirmed by neutron studies (see Ref. 17). The problem, however, remains controversial and in this paper the phrase “second-order transition” will be used in order to differentiate between two clearly different anomalies.
- ⁵⁷G. Subias, J. Garcia, J. Blasco, M. G. Proietti, H. Renevier, and M. C. Sanchez, *Phys. Rev. Lett.* **93**, 156408 (2004).
- ⁵⁸I. Leonov, A. N. Yaresko, V. N. Antonov, M. A. Korotin, and V. I. Anisimov, *Phys. Rev. Lett.* **93**, 146404 (2004).
- ⁵⁹Horng-Tay Jeng, G. Y. Guo, and D. J. Huang, *Phys. Rev. Lett.* **93**, 156403 (2004).